Proceedings of ICONE 8
8th International Conference on Nuclear Engineering
April 2-6, 2000, Baltimore, MD USA

ICONE-8319

STUDY OF SECOND PHASE PARTICLES IN ZR ALLOYS USING THE ADVANCED PHOTON SOURCE AT ARGONNE NATIONAL LABORATORY

K. T. Erwin
Department of Mechanical and Nuclear Engineering, The Pennsylvania State University
231 Sackett Building
State College, PA 16802
(814) 863-3644
(814) 865-8499
kte102@psu.edu

O. Delaire
Department of Mechanical and Nuclear Engineering, The Pennsylvania State University
231 Sackett Building
State College, PA 16802
(814) 863-3644
(814) 865-8499
oxd110@psu.edu

A. T. Motta
Department of Mechanical and Nuclear Engineering, The Pennsylvania State University
231 Sackett Building
State College, PA 16802
(814) 863-0036
(814) 865-8499
atm2@psu.edu

R. C. Birtcher
Materials Science Division,
Argonne National Laboratory,
MSD 212 E203
9700 S. Cass Ave
Argonne, IL 60439
(630) 252-4996
(630) 252-4289
birtcher@anl.gov

Y. S. Chu
Advanced Photon Source,
Argonne National Laboratory,
XFD 431 B006
9700 S. Cass Ave
Argonne, IL 60439
(630) 252-0150
ychu@aps.anl.gov

D. C. Mancini
Advanced Photon Source,
Argonne National Laboratory,
XFD 431 B008
9700 S. Cass Ave.
Argonne, IL 60439
(630) 252-0147
(630) 252-0161
mancini@aps.anl.gov

ABSTRACT

The types of precipitates present in zirconium alloys used for nuclear fuel cladding determine the cladding in-reactor behavior, especially corrosion resistance. The structure, size, distribution, and morphology of these precipitates depend on the alloy composition, thermo-mechanical treatment, and exposure to radiation. We examined the crystal structure of compounds in non-irradiated zirconium alloys using x-ray diffraction from the synchrotron radiation source at the Advanced Photon Source at Argonne National Laboratory (APS). The high brilliance and resolution of this light source allowed us to study very small (~0.1-0.2%) volume fractions of these second phases in the alloy. We examined four different alloys, two with well-known precipitate types and two with relatively unknown phases.

The results showed conclusively that x-ray diffraction analysis at the APS can be used to study these minute amounts of precipitates. To the authors' knowledge, this is the first time that these low-levels of precipitates in zirconium alloys were observed using a bulk diffraction technique. In the two well-known alloys (Zircaloy-4 and Zircaloy-2), we were able to identify all the phases reported (hcp C-14 $Zr(Cr, Fe)_2$ in Zircaloy 4 and Zircaloy-2 and C-16 bct $Zr_2(Ni, Fe)$ in Zircaloy-2). In the other alloys (ZIRLO and Valloy) we were able to identify new phases that either agree with other preliminary reports, or that are reasonably consistent with the alloy composition and relevant binary phase diagrams. We discuss the significance of these results as well as the future direction of this research, which will include the examination of neutron irradiated cladding samples.

KEYWORDS: ZIRCALOY, X-RAY DIFFRACTION, SYNCHROTRON, INTERMETALLIC PRECIPITATES, CORROSION

INTRODUCTION

Zirconium alloys are extensively used in the nuclear industry for nuclear fuel cladding, in part because of their superior corrosion resistance. The corrosion resistance of the zirconium

alloys used in nuclear applications is in turn determined by the alloy's second phase precipitate distribution, morphology, and composition. In particular, it is important to determine the types of precipitates present and their relative quantities as a function of the heat treatment and irradiation fluence. Many different mechanisms have been postulated to rationalize the influence that second-phase particles and/or alloying element content in the matrix have on the corrosion of these alloys. There is a considerable amount of data on the corrosion rates observed for different types and morphologies of second phase particles present. For example, a beta-quench heat treatment leading to small precipitates is known to improve the nodular corrosion resistance of Zircaloy 2 in BWRs and a large precipitate size distribution improves uniform corrosion resistance of Zircaloy 4 in PWRs [Garzarolli, 1992]. However, full mechanistic understanding of the influence of microstructure on the advancement of the corrosion layer in Zr alloys has not been achieved. Thus, although we understand empirically the effect of precipitate size on corrosion rate, we do not understand the mechanisms by which this occurs. Part of the problem is that we do not have a good estimate of the bulk volume fraction of intermetallic precipitates in the alloys as a function of heat treatment, and how this volume fraction changes with fluence. In this work, we attempt to measure this volume fraction directly using the synchrotron source.

It is particularly desirable to perform our studies of precipitate morphology in the bulk material, as then the problem of obtaining good statistics from TEM measurements of individual precipitates does not present itself. The difficulties that arise in measuring the volume fraction of the second phase precipitates are three fold. First, because of the relatively small amount of alloying elements in the matrix, the second phase particles volume fraction is very small (0.1~0.2%). Second, because Zr is a much heavier element than the alloying elements, the scattering intensity from the second phase particles are much weaker (they are roughly proportional to the second power of Z, total number of electrons per atom). Additionally, the diffuse scattering from the matrix contributes considerable background to the signal. Third, being a heavy element, the Zr matrix is an effective x-ray attenuator. For Cu-Kα radiation (8.042 keV), the attenuation length is only about 10 microns. Thus, both the incident and diffracted beam from the second phase particles suffer significant attenuation before the detection. Fig. 1 shows the powder diffraction pattern measured with a standard Cu-Kα x-ray source from one of the Zircaloy-4 samples later analyzed at APS. The only detectable peaks arise from the Zr-α matrix.

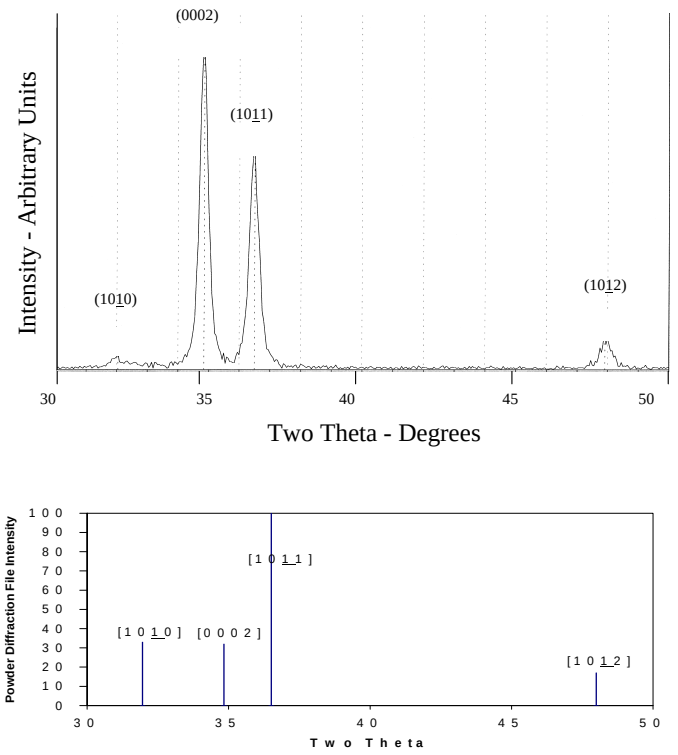

Figure 1. Zircaloy-4 X-ray Diffraction Pattern from Standard Diffractometer and Reported Powder Diffraction File Intensity for α-Zr.

A synchrotron radiation addresses all of the above problems by providing a much higher flux density (a factor of 100 or more depending on the beam optics) and energy-tunable capability. The increased flux density allows for more sampling of the second phase within the matrix. Thus, the data acquisition can be carried out much faster. The energy tuning ability allows a selection of a higher x-ray energy, which increases the penetration depth of the x-rays into the sample matrix. For example, the x-ray penetration at 13.5 keV is about 4.5 times larger than at 8 keV. Thus, the more incident photons can reach second phase particles and, likewise, escape out of the matrix into the detector, thereby increasing signal to background ratio.

This paper presents some of the initial studies aimed at obtaining bulk crystallographic information on the second phase particles in zirconium alloys, using synchrotron radiation.

1.0 Experimental Setup

The experiments were performed at the Advanced Photon Source synchrotron radiation facility located at Argonne National Laboratory in Argonne, Illinois. The data were collected at the number two bending magnet (2BM) beamline operated by the Synchrotron Radiation Instrumentation Collaborative Access Team (SRI-CAT).

Figure 2 shows a schematic diagram of this beamline. The incident beam energy of 13.533 keV (lambda = 0.09163 nm) was chosen in order to maximize the penetration of x-rays into the sample without sacrificing the x-ray flux due to optical constraints. The incident beam size was 1 mm (vertical) and 3 mm (horizontal). The diffracted beam was measured using a NaI scintillation detector with the vertical and horizontal acceptance of 1 mrad and 5 mrad, respectively. The diffraction measurements were carried out using a standard four-circle diffractometer.

Finally, in order to detect the weak diffraction intensity from the second phase, it is crucial that the measurements be performed in reciprocal space far away from the diffraction features of the matrix. Thus, we attempted to obtain x-ray diffraction patterns at angular locations away from any matrix peaks taking advantage of the textured nature of the matrix diffraction pattern when possible.

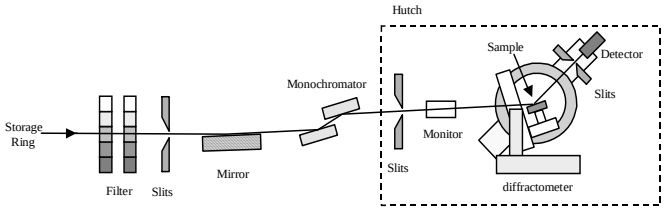

Figure 2. Experimental Setup of 2BM. The white x-ray beam (an x-ray spectrum of all wavelengths) is generated by synchrotron radiation. The apertured white beam is reflected off the Cr mirror, which serves as a low pass filter with the high-energy cut-off of 20 keV. A double crystal Si(111) monochromator selects a monochromatic x-ray beam with a bandwidth of about 2 eV. The monochromatic beam entering into a hutch (experimental station) was apertured down to reduced the background, and the diffraction measurements were performed using a standard four-circle diffractometer

1.1 Sample Preparation

The samples were cut using a standard diamond wheel cutting saw from either bulk sheet (Zircaloy-4, Zircaloy-2, and Valloy) supplied by General Electric Company, or tube (ZIRLO) supplied by Westinghouse Electric Corporation. The tube samples had been annealed in an argon atmosphere at 575°C for 2 hours in order to recrystallize the cold worked microstructure and increase precipitate size. The Zircaloy-2 and Valloy were subjected to a recrystallization heat treatment, which consisted of quenching from the β region (stability range is 863°C to 1455°C) at 50°C/s followed by three 15% cold working and annealing passes (total annealing time was 8h at 620°C). The Zircaloy-4 material was subjected to a precipitate growth heat treatment, which consisted of an α-phase heat treatment at 400°C for 48 hours following the standard Zircaloy-4 processing heat treatment. The samples were then polished on a mechanical milling machine using silicon carbide paper with a grit size of 35 μm followed by 15 μm. The final sample thicknesses varied from 300 to 700 μm.

2.0 Results and Discussion

In order to characterize the amount of alloying elements present in the sample, a chemical analysis was performed on each of the alloys by Luvak Inc. The results are listed in Table 1. Detection limits are between five and ten ppm for all elements. The values quoted for each alloy represent the average of three samples. The analyses were consistent from sample to sample.

The goal of the preliminary data analysis is to qualitatively identify the second phases present in the zirconium alloys. This will show that the technique can be applied to phase identification and analysis of small volume fraction second phases. After this has been completed, we will attempt to quantify from first principles the amount of second phase precipitates that exist in the samples. Spectra for each alloy are presented and analyzed below. Because the beam decays exponentially over time, the intensity is normalized against the incoming beam and thus is in arbitrary units.

Table 1. Chemical Analysis of Zirconium Alloys Used in This Work (Performed by Luvak Inc.)

Element	Zirc-2 (Wt. %)	Zirc-4 (Wt. %)	ZIRLO (Wt. %)	Valloy (Wt. %)
Iron	0.14	0.24	0.10	0.14
Chromium	0.11	0.11	0.001	1.35
Tin	1.55	1.64	1.08	<0.004
Nickel	0.063	0.0034	<0.001	<0.001
Oxygen	0.112	0.112	0.145	0.102
Nitrogen	0.003	0.002	0.005	0.003
Carbon	0.002	0.003	0.002	0.003
Silicon	0.0097	0.0095	0.013	0.015
Copper	0.0046	0.0020	0.0020	0.0016
Hafnium	<0.004	<0.004	<0.004	<0.004
Aluminum	0.0061	0.0058	0.012	0.020
Manganese	<0.001	<0.001	<0.001	<0.001
Molybdenum	<0.001	<0.001	<0.001	<0.001
Titanium	0.0020	0.0012	0.0019	<0.001
Tungsten	<0.004	<0.004	<0.004	<0.004
Niobium	---	---	1.23	---

2.1 Qualitative Results from X-ray Diffraction Patterns

The rolling texture obtained in as fabricated Zircaloy causes the α-Zr matrix peaks to depart from the reported powder diffraction intensities. During the thermomechanical treatment of the alloy, the basal planes align themselves with

the compressive stress direction and the prism planes align themselves with the rolling direction. This results in a texturing of the alloy, which increases the intensity of the basal poles relative to the pyramidal and prism poles for diffraction normal to the rolling surface. Of the four alloys that were analyzed, Zircaloy-2 and 4 have well-known second phase microstructures (Lemaignan, 1994 and Preble, 1998). These microstructures commonly consist of the $Zr(Fe,Cr)_2$ hexagonal (C14) or cubic (C15) Laves phases, the $Zr_2(Fe,Ni)$ body centered tetragonal (C16) phase, and at high Fe contents, the orthorhombic Zr_3Fe phase. These alloys were used as a calibration of the synchrotron instrument. By comparing the results obtained to alloys with known precipitates, we can determine if the data collected were accurate. The results show that the technique is sensitive enough to detect the precipitates on such a small level.

Figure 3 shows the x-ray diffraction pattern obtained for Zircaloy-4, along with the standard powder diffraction data for hcp C14 $Zr(Fe_{1.5}Cr_{0.5})$ (JCPDF file # 42-1289). All of the expected peaks are observed, although their relative intensities differ from the expected powder diffraction spectra. In particular, the (20$\underline{2}$1) reflection is diminished relative to the (11$\underline{2}$2) reflection. The (10$\underline{1}$3) reflection is on the shoulder of the large α-Zr peak and is thus not resolvable. The shift in relative intensities is likely due to the texture of precipitates in the matrix not being completely random. From the pattern, we can also determine that the lattice parameter of the C14 phase is close to the reported value of a=0.501 nm.

Preliminary examinations of Zircaloy-2 samples produced spectra that contain peaks that can be indexed as $Zr(Cr, Fe)_2$ and $Zr_2(Ni,Fe)$, although the texture effects appear to be more pronounced, and the peaks appear to be broadened, both of which are consistent with the smaller precipitate size in Zircaloy-2 as compared to Zircaloy-4. Further, the lattice parameters did not match exactly with the reported values of the $Zr(Cr, Fe)_2$ file mentioned above. It is well known that the lattice parameter of $Zr(Cr, Fe)_2$ changes with Fe/Cr ratio, and our energy dispersive x-ray analyses in the TEM have shown that Fe/Cr is lower than 3 in our samples. In addition, the precipitates in the matrix are subjected to compressive stresses that create defects (stacking faults) in the structure, all of which can affect the lattice parameter.

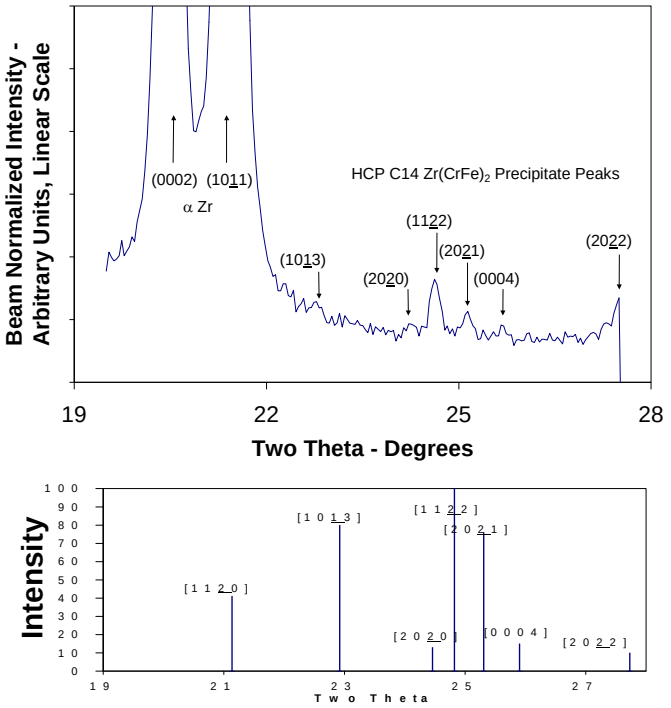

Figure 3. X-ray Diffraction Pattern from Zircaloy-4 and Reported Powder Diffraction File Intensity for $Zr(Fe_{1.5}Cr_{0.5})$ [JCPD 42-1289].

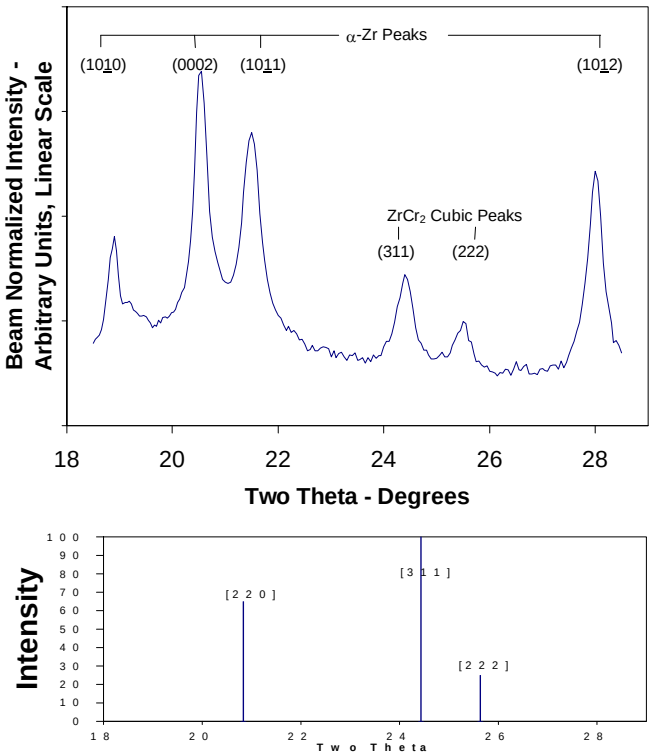

Figure 4. X-ray Diffraction Pattern from Valloy and Reported Powder Diffraction File Intensity for $ZrCr_2$ Cubic [JCPD 02-1108].

Further results were obtained from two other alloys analyzed, ZIRLO and Valloy. In both of these alloys, the crystal structures of the precipitates have not been fully characterized in the literature. Figure 4 shows the spectrum obtained for Valloy, a high Cr-content alloy developed by GE. The same texturing effects are visible for the α-Zr matrix. In addition, we see large peaks corresponding to the cubic C15 $ZrCr_2$ Laves phase (JCPDF file # 06-612). The volume fraction of second phase precipitates in this alloy is considerably larger than in Zircaloys, and the second phase peaks are correspondingly more intense. The observation of cubic $ZrCr_2$ is consistent with the Zr-Cr phase diagram at low temperature (i. e., this is the equilibrium phase) (Arias and Abriata, 1986).

The final alloy analyzed was ZIRLO. Figure 5 shows composite x-ray diffraction patterns plotted on the same graph (note that the vertical scale is linear). We can observe the peaks from both majority phases present (i. e., hcp α-Zr and bcc β-Nb). In addition to these, we can observe other peaks, arrowed at the bottom of the chart. Sabol et al. (1994) reported an hcp Zr-Nb-Fe phase with a=0.54 nm and c=0.87 nm; which is reasonably consistent with the values we obtained of a=0.508 nm and c=0.82 nm, and stoichiometries of Zr/(Nb+Fe)≈1 and Nb/Fe≈1. Other researchers have reported a hexagonal $Zr(Nb,Fe)_2$ phase (Shishov et al., 1996), but with a Zr/(Nb+Fe) of 0.5.

The above results are consistent with our preliminary TEM examinations as well as previous TEM work (Sabol, 1989 and Sabol 1994), in which we found two types of second phases, one containing Zr-Nb (β-Nb) and the second containing Zr-Nb-Fe. This experiment again demonstrates the ability of the technique to observe small volume fractions of second phase particles. One interesting result is the presence of the forbidden β-Nb [111] and [120] forbidden peaks. It is not yet known why these peaks appeared, but they could be due to some small deviation of the crystal structure that relaxes the forbidden conditions.

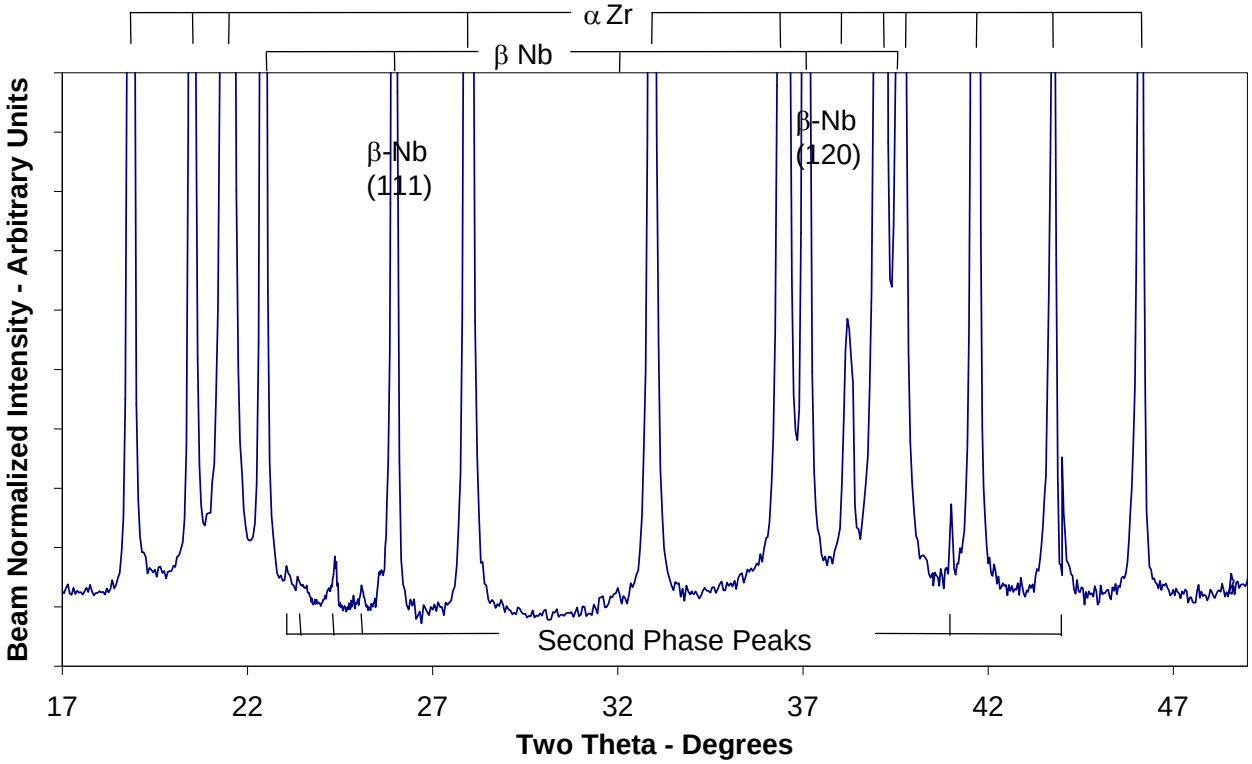

Figure 5. X-Ray Diffraction Pattern from ZIRLO with Various Phases (β-Nb, α-Zr, and Second Phase Particles) indicated.

2.2 Quantitative Analysis of X-Ray Diffraction Patterns

These data will be quantitatively analyzed in order to obtain reasonable estimates of second phase densities. These results will be compared to calculations of precipitate densities from first principles assuming that all of the alloying elements are in the form of second phases, and also to TEM work.

3.0 Conclusions

Using the high brilliance, high resolution, and energy tunable characteristics of the x-ray source, we have demonstrated for the first time that we can detect small amounts of second phase particles (0.1-0.2 wt%), which were previously not examinable using bulk x-ray diffraction.

Further, results have shown agreement with the expected microstructures of two well-characterized alloys, Zircaloy-2 and Zircaloy-4. For two alloys in which the precipitate structure was less well known, our measurements yielded results that were consistent with the existing phase equilibria information. This has the potential of enabling more detailed studies of precipitate growth and aging processes in the bulk.

Future work will include quantifying the amount of second phases from the x-ray diffraction patterns, and the comparison of this quantification to expected second phase amounts from calculations and literature values. Finally, neutron irradiated samples will be examined at the APS, enabling the effects of irradiation on the second phase particle morphology to be better understood.

ACKNOWLEDGMENTS

Thanks are due to R. B. Adamson at G.E. Vallecitos, and R. J. Comstock at Westinghouse Science and Technology Center for furnishing the samples used in this study. Further, A. T. Motta would like to acknowledge helpful discussions with R. J. Comstock. We also wish to thank B. Kestel at ANL MSD for his expert preparation of TEM samples. Use of the Advanced Photon Source was supported by the U.S. Department of Energy, Basic Energy Sciences, Office of Science, under Contract No. W-31-109-Eng-38. This research was sponsored by the Department of Energy, Nuclear Engineering Education and Research (DOE-NEER) program, under grant number DE-FG07-98ID 13637.

REFERENCES

Arias, D., and Abriata, J. P., (1986), in Bull. Alloy Phase Diagrams, 7(3), pp. 237-243.

Cheng, B., Gilmore, P. M., and Klepfer H. H., "PWR Zircaloy Fuel Cladding Corrosion Performance, Mechanisms and Modeling," Zirconium in the Nuclear Industry: Eleventh International Symposium, ASTM STP 1295, E. R. Bradley and G. P. Sabol, Eds., American Society for Testing and Materials, Philadelphia, 1996 pp. 137-160.

Garzarolli, F. and Holzer, R., "Waterside Corrosion Performance of Light Water Power reactor Fuel," Journal of the British Nuclear Society 31: (1) Feb 1992, pp. 65-85.

Lemaignan, C. and Motta, A. T., "Zirconium Alloys in Nuclear Applications" Vol 10B, Materials Science and Technology Series, Ed. by B. R. T. Frost, VCH, New York, 1994, pp. 1-51.

PCDPDFWIN v. 2.01, (1998) JCPDS-International Center for Diffraction Data, Newtown Square, PA.

Preble E. A. and Murty K. L., (1998), "A Review of Intermetallic Precipitates and Their Influence on Zircaloy Corrosion in Nuclear Reactors," CORCON-97: Corrosion and Its Control. II; Elsevier Science BV, pp. 609-614.

Sabol, G. P., Comstock, R. J., Weiner, R. P., Larouere, P., Stanutz, P. N., (1994), "In-reactor Corrosion Performance of ZIRLO and Zircaloy-4," Zirconium in the Nuclear Industry: Tenth International Symposium, ASTM STP 1245, A. M. Garde and E. R. Bradley, Eds., American Society for Testing and Materials, Philadelphia, pp. 724-744.

Sabol, G. P., Kilp, G. R., Balfour, M. G., and Roberts, E., (1989), "Development of a Cladding Alloy for High Burnup," Zirconium in the Nuclear Industry: Eighth International Symposium, ASTM STP 1023, L. F. P. Van Swam and C. M. Eucken, Eds., American Society for Testing and Materials, Philadelphia, pp. 227-244.

Shishov, V. N., Nikulina, A. V., Markelov, V. A., Peregud, M. M., Kozlov, A. V., Averin, S. A., Koblenkov, S. A., and Novoselov, A. E., (1996), "Influence of Neutron Irradiation on Dislocation Structure and Phase Composition of Zr-Base Alloys," Zirconium in the Nuclear Industry: Eleventh International Symposium, ASTM STP 1295, E. R. Bradley and G. P. Sabol, Eds., American Society for Testing and Materials, pp. 603-622.